

THE EFFECT OF RESIDUAL STRESSES AND STRAINS ON FATIGUE CRACK PROPAGATION: MEASUREMENT AND MODELLING

D. Nowell, L.J. Fellows, D.A. Hills, and Y. Xu

Department of Engineering Science, University of Oxford,
Parks Road, Oxford, OX1 3PJ, UK

ABSTRACT

Moiré interferometry provides an accurate means of measuring residual displacements around a propagating fatigue crack. From these displacements, crack closure behaviour and residual stresses may be determined. This paper describes the construction and operation of an in-situ moiré interferometer, mounted on a servohydraulic fatigue machine. Photoresist gratings were applied to fatigue specimens of Ti 6/4 and these proved durable under fatigue loading. Crack closure data is presented for a number of loading conditions, including constant amplitude loading and a single overload cycle. The results obtained are compared to the predictions of a plane stress boundary element model, based on the concept of strip yield. Encouraging agreement is obtained, particularly for the case of constant amplitude loading.

KEYWORDS

Fatigue, crack closure, residual stress, moiré interferometry.

INTRODUCTION

It has long been recognised that plasticity in the region of the crack tip is an important aspect of the fatigue process in most engineering materials. The existence of such regions of plasticity implies that there are also residual stresses and strains close to the crack tip and, in the case of a propagating fatigue crack, these remain behind as the crack grows so that a region of residually strained material exists along the crack flanks. Elber [1,2] was the first to report the phenomenon of plasticity-induced crack closure where, even in purely tensile loading, the tip of a fatigue crack is found to be closed for part of the loading cycle. This phenomenon is important, since it provides a means of explaining experimental observations that crack growth rate depends on loading history as well as nominal ΔK . In order to exploit this phenomenon for improved predictions of crack propagation life, two key techniques are required:

- (i) A convenient and accurate means of measuring crack closure, residual stresses, and residual strains for cracks under controlled loading.
- (ii) A model which is sufficiently detailed to predict the important aspects of the observed behaviour, yet simple enough to allow modelling of representative loading histories in a reasonable timescale.

Techniques have not yet been developed which can fully meet these requirements, but a range of approaches are now available which can go some way towards the objectives. Traditional means of monitoring crack

closure, such as compliance measurements with crack mouth gauges or strain gauges, electrical resistance, etc have now been complemented by full field techniques such as moiré interferometry [3] or photoelasticity [4]. Moiré provides surface information only, but in principle may be applied to any material. Photoelasticity does offer the possibility of through thickness measurements, but only for a restricted range of materials. Thus, for use on engineering materials, moiré interferometry provides the best current technique for obtaining full field displacement measurements, although alternatives such as laser speckle interferometry are under investigation. Modelling of fatigue crack closure can be carried out using finite element methods [5], but the computational resources required for simulation of practical load cycles have led to the development of simplified boundary element methods such as that proposed by Newman [6]. These simplified models often use an approximation for the basic plasticity mechanism such as the Dugdale strip yield assumption [7].

The current paper describes work carried out on the aerospace alloy Ti-6Al-4V. Full-field displacement measurements were made around the tip of a growing fatigue crack using moiré interferometry. From these it was possible to determine residual strains and crack opening. A simple boundary element model was then used to compare the experimental measurements with predictions.

EXPERIMENTAL WORK

Fatigue cracks were grown in small 4-point bend specimens of Ti-6Al-4V. Specimens were 8mm deep by 7mm thick and the inner and outer support spacing was 60mm and 110mm respectively. In order to measure the displacements at any point of the fatigue cycle (including cycles with positive R-ratio), an in-situ interferometer was built adjacent to the servo-hydraulic fatigue machine. The design and operation of the interferometer is described fully by GÜNGÖR and FELLOWS [8]. Interference gratings of 1200 lines per mm were applied to the surface of the specimen to give a displacement sensitivity of $0.417\mu\text{m}$ per fringe order. In our earlier work [3], these were applied using a standard replication technique to produce aluminium gratings bonded by an epoxy resin. It was found in practice that the quality of these gratings deteriorated quite rapidly with fatigue cycling, usually by debonding of the adhesive, so that they were not suitable for tracking the specimen through a number of load cycles. An improved grating system was therefore developed based on a polymer photoresist (Hunts 514 [8]). The photoresist was applied to the specimens by dipping and then exposed to a laser interference pattern in order to produce the grating. After development the gratings were coated with a thin layer of gold to improve reflectivity. Interference patterns were collected by the temporal phase-stepping method [9], giving values of intensity $I(x,y)$ at each spatial point in the region of interest for five different phase differences, δ_i . Data was collected from a 256×256 array over a region close to the crack tip, with a pixel spacing of about $9\mu\text{m}$. Determination of the phase, ϕ , of the interference pattern at each point was carried out by a least squares technique using the equation

$$I_i(x,y) = a(x,y) + b(x,y)\cos(\phi(x,y) + \delta_i) \quad (1)$$

where $a(x,y)$ is the local background intensity and $b(x,y)$ is the contrast. Values of ϕ vary between $-\pi$ and π between one fringe order and the next. An unwrapping routine [10] is therefore used to determine absolute phase, from which the u or v displacement component can be obtained. The displacements need to be measured relative to an arbitrary datum and, in our experiments, the interferometer was adjusted to give a null field at the lowest load in the cycle. Displacements of opposite sides of the crack line could then be monitored at a number of steps during the loading cycle. Any increase in relative displacement of the two crack faces was interpreted as an opening of the crack.

MODELLING

Modelling of crack behaviour was carried out using a boundary element strip yield model which is physically similar to Newman's [6]. The principal innovation in the model was the use of a quadratic

programming formulation [11] which automatically determined the appropriate boundary condition in each region, i.e. along the crack faces:

$$\sigma_{xx} = 0, \quad b > 0, \quad (\text{Crack open}) \quad (2)$$

$$\sigma_{xx} < 0, \quad b = 0, \quad (\text{Crack closed}) \quad (3)$$

where b is the crack opening, and within the yield zone:

$$\sigma_{xx} = \sigma_y, \quad \Delta b > 0, \quad (\text{Tensile yield}) \quad (4)$$

$$-\sigma_y \leq \sigma_{xx} \leq \sigma_y, \quad \Delta b = 0, \quad (\text{No yield}) \quad (5)$$

$$\sigma_{xx} = -\sigma_y, \quad \Delta b < 0, \quad (\text{Compressive yield}) \quad (6)$$

Here, Δb is interpreted as the change in plastic displacement in the yield strip during the current load step and σ_y is the yield stress. The material is modelled as elastic/ideally plastic. Several hundred elements are used along the crack and in the yield strip and a focussed mesh is employed so that greater definition is obtained close to the crack tip. Typical output from the model is shown in Figure 1, where σ_{xx} and crack shape are plotted along the crack line ($x = 0$). Full field displacements and stresses may also readily be obtained.

RESULTS

A range of results were collected for different load conditions as shown in Table 1.

TABLE 1
LOAD CONDITIONS INVESTIGATED

Test No	Ref. No	Maximum Load (P_{\max}/P_y)	Minimum Load (P_{\min}/P_y)	Overload (P_{ovl}/P_y)	R-Ratio	Crack Length (mm)
1	17	0.529	0.0	-	0.0	0.842
2	17a	0.529	0.0	-	0.0	1.704
3	22	0.529	-0.529	-	-1.0	1.040
4	55	0.705	0.282	-	0.4	1.235
5	51	0.529	0.0	0.881	0.0	0.438
6	53	0.265	0.0	0.529	0.0	1.881

Loads given in the table have been normalised with respect to P_y , the load required to produce first yield in an uncracked specimen.

Constant amplitude loading

Tests 1 to 4 were carried out by subjecting the specimen to constant amplitude loading. Cracks initiated and grew from a starter notch and, since the remote load was constant, were subject to a slowly increasing ΔK . At an appropriate crack length a series of moiré interferograms were taken at different loads during the cycle, both during the loading and the unloading parts. The discontinuity in displacement across the crack was extracted from the raw displacement data and plotted against position along the crack for each load step. It should be remembered that the initial grating was applied to the undeformed and uncracked specimen. Thus, the displacement data collected at the minimum load step incorporates residual deformation caused by

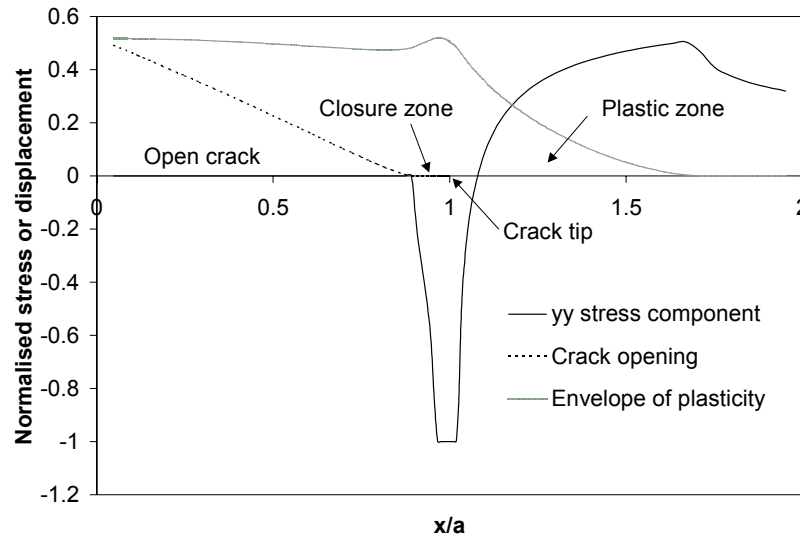


Figure 1: Typical output from boundary element model for a partially-closed crack, $R = 0.0$, $P_{max}/P_y = 0.6$, constant amplitude load.

crack tip plasticity as the crack grows. Grating damage was observed close to the crack faces, so that the displacement could not be measured right up to the crack face. Consequently there was some displacement discontinuity across the crack even at zero load when portions of the crack might be expected to be closed. The following procedure was therefore adopted to determine the extent of crack closure.

- (i) Moiré displacement data was collected at n load steps during the loading cycle
- (ii) For each load step i , the displacement discontinuity $\delta_i(x)$ across the crack was determined and plotted against position along the crack
- (iii) For $i > 0$, the change in displacement discontinuity from minimum load, $d_i(x)$ was calculated by subtracting the value at minimum load, $\delta_0(x)$. i.e. $d_i(x) = \delta_i(x) - \delta_0(x)$.
- (iv) Where $d_i(x)$ was found to be close to zero it was assumed that the crack faces had not moved relative to each other since minimum load and that the crack was therefore closed in this region.

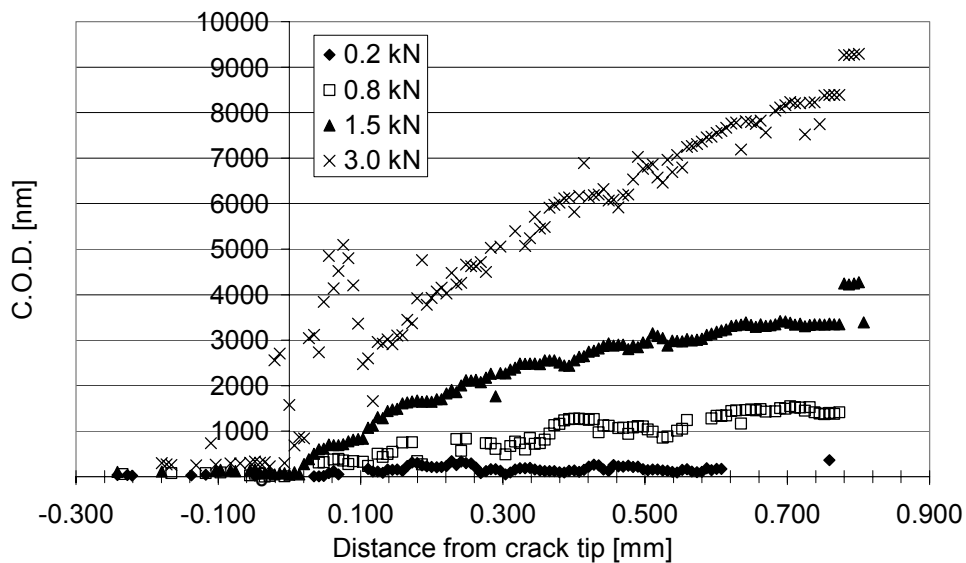


Figure 2: Measurements of crack face displacement during loading phase (test 1)

Typical output data from this procedure is shown in Figure 2, for Test 1 during the loading half of the cycle. It may be seen that the crack is closed at the tip until a load of 1.5kN is applied. Some evidence of crack tip

opening displacement is visible at maximum load, although this is partly obscured by excessive scatter in the data points close to this region. Figure 3 shows the corresponding output from the model. It can be seen that there is surprisingly good agreement between the experimental data and model predictions. Figure 4 shows the variation of percentage of the crack which is open against load for the same test. Tests 2, 3, and 4 show a similar pattern of agreement between experiment and model.

Overload tests

Some difficulty was experienced in carrying out the overload tests due to crack branching which occurred at the higher load levels. Nevertheless, some useful data were obtained. Figure 5 shows crack shape immediately after the overload. Both experimental data and the model predict that the crack is fully open in this case. It should be noted that the apparent difference between model predictions and measurements ahead of the crack tip is a consequence of the concentration of plasticity in a thin strip in the model, whereas in reality it is distributed over the entire plastic zone. The overloaded crack was then grown on and displacement readings taken at crack lengths of 0.654, 0.700, 0.916, and 1.158 mm. Even for the longest of these, normal closure behaviour had not been re-established.

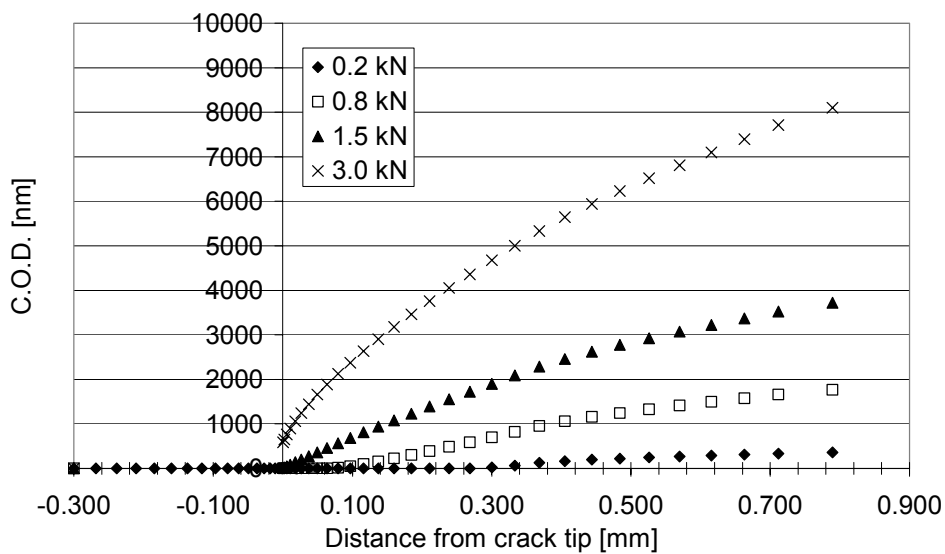


Figure 3: Predictions of crack face displacement from the model, corresponding to the measurements shown in Figure 4.

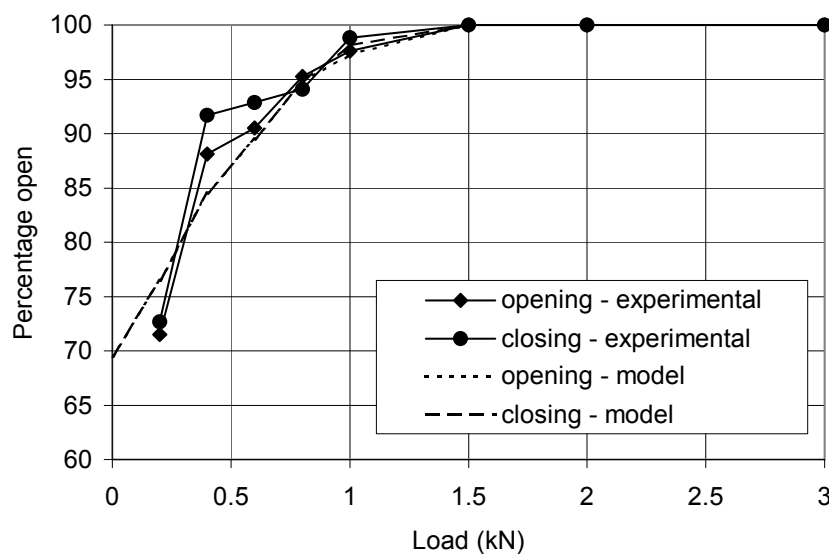


Figure 4: Variation of proportion of crack open with load for test 1

DISCUSSION AND CONCLUSIONS

Model predictions and experimental measurements of crack profiles show surprisingly good agreement for constant amplitude loading. Predictions of the distribution of strain ahead of the crack are, of course, much less satisfactory, due to the concentrated plasticity assumptions inherent in the strip yield model. The model is appropriate to a two-dimensional plane stress situation. Although the moiré displacement readings are taken on the surface, it should be remembered that the specimen is fully three-dimensional and the surface displacements will be influenced by conditions remote from the surface. The agreement between the model and experimental data is less satisfactory for the single overload tests carried out. This may be due to the higher levels of plasticity involved during the overload cycle, which can be less satisfactorily modelled using the strip yield assumption. However, the experimental data does demonstrate that, as predicted by the model, the effects of an overload persist, even when the crack tip has completely traversed the overload plastic zone. Overall the predictions of the model are encouraging and suggest that such simplified models might form the basis of enhanced life prediction methods. More work needs to be done, however, particularly in understanding three-dimensional effects, since most real cracks contain a portion of the crack front which is essentially plane strain.

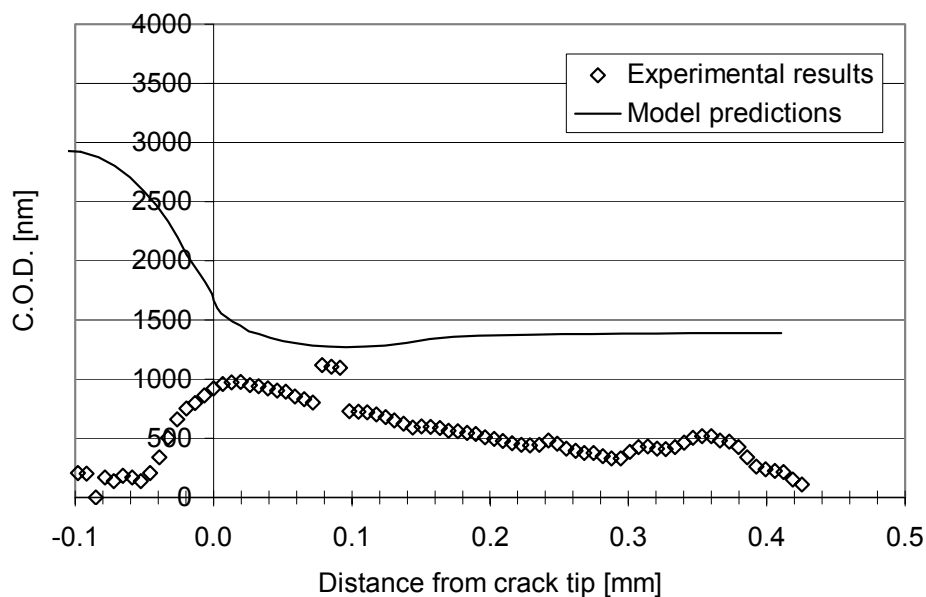


Figure 5: Crack face displacement for test 5 immediately after overload at zero load

REFERENCES

1. Elber, W. (1970). *Eng. Fract. Mech.* 2, 37.
2. Elber, W. (1971). In: *Damage tolerance in aircraft structures*, ASTM STP 486, pp 230-247. ASTM, Philadelphia.
3. Fellows, L.J., Nowell, D., and Hills, D.A., (1997). In: *Advances in Fracture Research*, pp 2551-2558, Karihaloo B.L., Mai, Y-W, Ripley, M.I., and Ritchie, R.O., Eds, Pergamon, Oxford.
4. Pacey, M.N., Patterson, E.A., and James, M.N. (2001). *Proc. Roy. Soc.*, under review.
5. Chermahini, R.G. and Blom, A.F., (1991). *Theoretical and Applied Fracture Mechanics*, 15, 267.
6. Newman, J.C. Jr., (1981). In: *Methods and models for predicting fatigue crack growth under random loading*, ASTM STP 748, pp53-84, Chang J.B., and Hudson, C.M., Eds. ASTM, Philadelphia.
7. Dugdale, D.S. (1960). *Jnl Mech. Phs. Solids*, 8, 100.
8. GÜNGÖR, S., and Fellows, L. (1998) In: *Experimental Mechanics: Advances in Design, Testing, and Analysis*, pp1071-1076, Allison, I.M., Ed, Balkema, Rotterdam.
9. Poon, C.Y., Kujawinska, M., and Ruiz, C., (1993). *Exp. Mech.*, 33, 234.
10. Takeda, M., Ina, H., and Kobayashi, S. (1982). *Jnl Opt. Soc. Amer.*, 72, 156.
11. Nowell, D., (1998) *Fatigue and Fract. of Eng Mats and Structs*, 21, 857-871.